DETECTION OF GRB 090618 WITH *RT*-2 EXPERIMENT ONBOARD THE *CORONAS − PHOTON* SATELLITE

A. R. Rao[1], J. P. Malkar[1], M. K. Hingar[1], V. K. Agrawal[1,2], S. K. Chakrabarti[3,4], A. Nandi[2,4], D. Debnath[4], T. B. Kotoch[4], R. Sarkar[4], T. R. Chidambaram[5], P. Vinod[5], S. Sreekumar[5], Y. D. Kotov[6], A. S. Buslov[6], V. N. Yurov[6], V. G. Tyshkevich[6], A. I. Arkhangelskij[6], R. A. Zyatkov[6], Sachindra Naik[7]

ABSTRACT

We present the results of an analysis of the prompt gamma-ray emission from GRB 090618 using the *RT*-2 Experiment onboard the *Coronas − Photon* satellite. GRB 090618 shows multiple peaks and a detailed study of the temporal structure as a function of energy is carried out. As the GRB was incident at an angle of 77° to the detector axis, we have generated appropriate response functions of the detectors to derive the spectrum of this GRB. We have augmented these results using the publicly available data from the *Swift* BAT detector and show that a combined spectral analysis can measure the spectral parameters quite accurately. We also attempt a spectral and timing analysis of individual peaks and find evidence for a systematic change in the pulse emission characteristics for the successive pulses. In particular, we find that the peak energy of the spectrum, E_p, is found to monotonically decrease with time, for the successive pulses of this GRB.

Subject headings: gamma-rays burst: general — instrumentation: detectors — supernovae: general

1. INTRODUCTION

Gamma-ray bursts (GRBs) are very fascinating cosmic objects in the universe. Since its discovery in 1973 (Klebesadel et al. 1973), GRBs opened up a new domain of astrophysical research due to the rich observational characteristics of the afterglows in a vast range of electromagnetic spectrum from γ-rays to radio wavelengths (see Gehrels et al. 2009 for a review). There is a general consensus in the literature that the diverse observational characteristics are due to the interaction of relativistic matter with the surrounding medium. The nature and energy source for this relativistic matter, particularly in the context of the long GRBs, could be in the nature of bulk motion of ions (the Fire Ball Model - see e.g., Piran 2004), cannon balls emitted from a compact object newly formed in a supernova explosion (Dar 2006), or particles accelerated by magnetized winds (the electro-magnetic model - see Lyutikov 2006 and references therein). The long GRBs are associated with supernovae and it is believed that relativistic matter of very high bulk Lorentz factor is generated in a conical jet during the collapse of a massive star at cosmological distances (see for example, Meszaros 2002). The prompt gamma-ray emission has several characteristic correlations like the peak energy E_p against the isotropic luminosity E_{iso} (Amati et al. 2002), spectral lag against the peak luminosity (Norris et al. 2000) etc. (see Gehrels et al. 2009, for a summary of such correlations) and these relations are used even in predicting the red shift of long duration gamma-ray bursts, although with a large uncertainty (close to a factor of 2, see, for example Xiao & Schaefer 2009). A detailed understanding of the prompt emission is necessary to put these correlations in a firm footing so that GRBs can be used as cosmological candles and also to have a clear understanding of the central engine and the basic jet/cannon-ball emission mechanism.

The morphology or temporal profile of the GRBs during the prompt emission varies asymmetrically with no apparent structure among the bursts. Some GRBs show multiple pulses and the individual pulses in a burst is a separate and unique emission with varying amplitude and intensity. In the frame work of Fireball Model (see, Zhang 2007 and Meszaros 2002 for reviews) these pulses are created with different shock strengths at different locations of the jet. Observations suggest that in most of the bursts, an individual pulse profile is in the shape of fast-rise-exponential-decay (FRED), with the width decreasing with energy (Fenimore et al. 1995; Norris et al. 2005). Spectral lag is another spectro-temporal property which is crucial to understand the dynamics and energetics of GRBs and can constrain the GRB models (Ioka & Nakamura 2001; Shen et al. 2005; Lu et al. 2006).

GRB 090618 is a very interesting object for several reasons. It is bright and relatively nearby (redshift $\sim$ 0.5) making it a good candidate to expect to have a visible supernova (if it is like SN1998bw - see Dado & Dar 2010), though no supernova has yet been associated with this GRB. Further, its intense hard X-ray and gamma-ray emission during the prompt phase enables one to make a time resolved spectral analysis (see for example, Ghirlanda et al. 2010). In this paper, we make a detailed analysis of the prompt emission in a wide band X-ray and gamma-ray region using data from Swift/ BAT and the *RT*-2 Experiment onboard the *Coronas − Photon* satellite (preliminary results are given in Rao et al. 2009). Since this is the first result from this experiment, we describe in detail the methodology used in deriving the response matrix and spectral fitting. We augment our

[1] Tata Institute of Fundamental Research, Mumbai - 400005, India. *arrao@mailhost.tifr.res.in*
[2] Space Science Division, ISRO-HQ, New Bell Road, Bangalore - 560231, India
[3] S. N. Bose National Center for Basic Sciences, Salt Lake, Kolkata - 700098, India
[4] Indian Center for Space Physics, Garia, Kolkata - 700084, India
[5] Vikram Sarabhai Space Center, VRC, Thiruvananthapuram - 695022, India
[6] Moscow Engineering Physics Institute, Moscow - 115409, Russia
[7] Astronomy & Astrophysics Division, Physical Research Laboratory, Ahmedabad - 380009, India

results by using the publicly available *Swift* BAT data and make a combined spectral fit. We examine the spectral and temporal characteristics of the individual pulses during the prompt emission of this GRB and investigate the implications to the source emission mechanisms. In §2, a summary of observations on GRB 090618 is given and in §3 a brief description of the *RT*-2 Experiment is given. Observations and analysis results (*RT*-2 and BAT data) are given in §4 and finally in §5, a discussion of the results are presented along with relevant conclusions.

2. GRB 090618

The bright and long gamma-ray burst GRB 090618 was discovered with the *Swift* Burst Alert Telescope (BAT) on 2009 June 18 at 08:28:29 UT (Schady et al. 2009a; 2009b; 2009c) at a red shift of z=0.54 (Cenko et al. 2009b). The GRB was detected by various observatories in X-ray and gamma-ray energies such as AGILE (Longo et al. 2009), Fermi GBM (McBreen et al. 2009), Suzaku WAM (Kono et al. 2009), Konus-Wind onboard Wind satellite and Konus-RF onboard Coronas-Photon satellite (Golenetskii et al. 2009), *RT*-2 Experiment onboard Coronas-Photon satellite (Rao et al. 2009) etc. The optical afterglow of GRB 090618 was soon detected with the Katzman Automatic Imaging Telescope (KAIT) (Perley et al. 2009), ROTSE-IIIb (Rujopakarn et al. 2009), Palomar 60-inch telescope (Cenko et al. 2009a) and various other optical, infra-red and radio observatories.

The X-ray afterglow of GRB 090618, as measured by the *Swift* XRT (Schady et al. 2009c), was very bright in X-rays, initially. Soon after, the flux decayed rapidly with a slope of ∼6 before breaking at T_0+310 s (T_0 = 08:28:29 UT) to a shallower slope of 0.71±0.02 (Beardmore et al. 2009). Further breaks at longer time scales were also reported (Schady et al. 2009c). Spectral fitting to the *Swift* data in the range of T_0+250 s and T_0+1065 s with a power law model modified by interstellar absorption yielded a photon index of ∼2 and the intrinsic absorption of 1.78×10^{21} cm^{-2} (Beardmore et al. 2009). They estimated the 0.3-10 keV unabsorbed flux to be 1.16×10^{-9} erg cm^{-2} s^{-1}.

Significant spectral evolution was observed during the prompt emission of the burst. Time-averaged spectrum from T_0-4.4 to T_0+213.6 s was well fitted by a power law with an exponential cut-off with photon index of 1.42 and E_p of 134 keV (Sakamoto et al. 2009). Time-integrated 20 keV – 2 MeV spectra obtained from the Konus-Wind (from T_0 to T_0+142 s; T_0 = 08:28:24.974 UT) onboard Wind satellite and Konus-RF (from T_0 to T_0+142 s; T_0 = 08:28:27.060 UT) instrument onboard Coronas-Photon satellite when fitted by GRB (Band) model, provided the values of the low-energy photon index (α), high-energy photon index (β) and peak energy (E_p) to be -1.28, -2.66, 186 keV (for Konus-Wind) and -1.28, -3.06, 220 keV (for Konus-RF), respectively (Golenetskii et al. 2009). The BAT light curve of the GRB was found to be of a multi-peak structure with a duration of about 130 s. The time-averaged BAT spectrum from T_0-5 to T_0+109 s can be described by simple power-law model with index ∼ 1.7 (Baumgartner et al. 2009). The fluence in the 15-150 keV band is $1.06 \pm0.01 \times 10^{-4}$ erg cm^{-2}. The multi-peaked profile was also seen in the 50 keV – 5 MeV range light curve obtained from the Suzaku Wide-band All-sky Monitor (Kono et al. 2009).

Ukwatta et al. (2010) derived the spectral lag of this GRB using the Swift BAT data and found that it supports the existence of a lag-luminosity relation. Ghirlanda et al. (2010) investigated the time resolved spectral characteristics of several GRBs using Fermi data and concluded that the E_p – L_{iso} relation holds good during the rising and decaying phases of pulses for a few GRBs, particularly for GRB 090618.

3. *RT*-2 EXPERIMENT ONBOARD THE CORONAS-PHOTON SATELLITE

The *RT*-2 Experiment (RT - Roentgen Telescope), which is a part of Indo-Russian collaborative project of Coronas-Photon mission (Kotov et al. 2008; Nandi et al. 2009), is designed and developed for the study of solar hard X-rays in ∼15 keV to 100 keV energy range. This experiment consists of three instruments (two phoswich detectors called *RT*-2/S and *RT*-2/G, and one solid-state imaging detector *RT*-2/CZT) and one processing electronic device (*RT*-2/E). The *RT*-2/S and *RT*-2/G detector assembly consist of NaI(Tl) / CsI(Na) scintillators in phoswich assembly viewed by a photomultiplier tube (PMT). Both the detector assemblies sit behind respective mechanical slat collimators surrounded by a uniform shield of Tantalum material and having different viewing angles of 4°×4° (*RT*-2/S) and 6° × 6° (*RT*-2/G). The *RT*-2/S covers ∼15 keV to 100 keV, extendable up to 1 MeV, whereas the use of an Aluminum (Al) filter in *RT*-2/G sets the lower threshold at ∼ 20 keV. The *RT*-2/CZT consists of three CZT detector modules (OMS40G256) and one CMOS detector (RadEye-1) arranged in a 2×2 array. Each CZT module consists of 256 individual detectors (pixel dimension of 2.5 mm × 2.5 mm), which are controlled by 2 ASICs. The CMOS detector consists of 512×512 pixels of individual pixel dimension of 48 μm. The entire CZT-CMOS detector assembly is mounted behind a collimator with two different types of coding devices, namely coded aperture mask (CAM) and Fresnel zone plate (FZP), surrounded by a uniform shield of Tantalum material and has varying viewing angles of 6′–6° depending on different configurations of the collimator (Nandi et al. 2010). The *RT*-2/CZT payload is the only imaging device in the Coronas-Photon mission to image the solar flares in hard X-rays in the energy range of 20 to 150 keV. All three-detector systems are interfaced with the satellite system (called SSRNI) through *RT*-2 Electronic processing payload (*RT*-2/E). The *RT*-2/E receives necessary commands from the satellite system and passes it to the individual detector system for proper functionality of the detector units and acquires data from the detector system and stores in its memory for further processing.

The mission was successfully launched from Plesetsk Cosmodrome, Russia on 2009 January 30. To maximize the Sun observation time, the satellite was put into a low earth (500 km) Sun-synchronous near-polar (inclination 82.5°) orbit. The test and evaluation results of this payload are described in Debnath et al. (2010), Kotoch et al. (2010), Nandi et al. (2010), Sarkar et al. (2010) and Sreekumar et al. (2010). Some details of the experiment can also be found at http://csp.res.in/rt2-main.html.

4. OBSERVATION AND ANALYSIS

4.1. *RT-2 Observations*

During the GRB event, the *RT*-2 payload was completely in the 'SHADOW' mode (away from the Sun) which started at 08:16:10.207 UT and ended at 08:37:35.465 UT. GRB 090618 was detected by the *RT*-2 instruments (Rao et al. 2009) with a large off-axis angle of 77°. Data from *RT*-2/S and *RT*-2/G are used for the present analysis. The scientific data from the detectors were stored in the memory of *RT*-2/E and then compressed using the onboard software before being transferred to the satellite system (known as SSRNI) for downlink to the ground station. During the 'SHADOW' mode, the spectra are accumulated every 100 s (see the spectral analysis section) and eight channel count rates (for each detector) are accumulated every 1 sec. These eight channels are divided equally between the 15 – 100 keV data from the 3 mm thick NaI(Tl) detector and the 26 – 1000 keV data from the 25 mm thick CsI(Na) detector, operated in a Phoswich mode. For the present work, we use the latter four channel data, which have the ranges of 26 – 59 keV, 59 – 215 keV, 215 – 330 keV, and 330 – 1000 keV, respectively.

The 'SHADOW' mode data of *RT*-2/S and *RT*-2/G detectors of 'GOOD' time (away from high background regions) span of $\sim$ 800 s from 08:23:27 UT to 08:36:47 UT were analyzed. During this time, the satellite was completely away from both the polar cap and high background SAA regions. GRB 090618 was detected by both the scintillator detectors. The light curves of 1 s time resolution were generated from the data obtained from both the detectors at different energy bands. Spectral data of 100 s, during the present GRB event, were also analyzed to study the evolution of the GRB spectrum.

4.2. *Swift BAT Observations*

Burst Alert Telescope (Barthelmy et al. 2005) onboard the *Swift* mission (Gehrels et al. 2004) is a highly sensitive, large field of view instrument, primarily designed to monitor the sky to detect gamma-ray events. It consists of an array of CdZnTe detectors, located behind a coded aperture mask. *Swift* also has an X-ray Telescope (XRT; Burrows et al. 2005) and UV/Optical Telescope (UVOT; Roming et al. 2005) which can make follow up observations within a few hundred seconds after the trigger.

BAT registered GRB 090618, triggered at 08:28:29 UT. The BAT position of the burst with $3'$ uncertainty is RA(J2000), Dec(J2000) = 294.021, +78.353 (Schady et al. 2009a). Astrometrically corrected position using Swift-XRT data and Swift-UVOT data is RA(J2000), Dec(J2000) = 293.99465, +78.35677 (Evans et al. 2009; Schady et al. 2009c). We have analyzed the Swift BAT data to understand the prompt emission from this GRB.

We used **heasoft6.5.1** for our analysis. First we created the detector plane image using the task *batbinevt* and then the detector mask file was created using task *batdetmask*. The quality map file was created using task *bathotpix*. Mask weighting using new XRT and UVOT position to BAT data was applied using task *batmaskwtevt*. Then mask weighted light curves were generated using task *batbinevt*. The GRB light curve shows multi-peaked structure with a precursor and the main burst starts at T_0+50 s. We generated light curves for the full burst (T_0 to T_0+180) in 4 energy bands: 15-25 keV, 25-50 keV, 50-100 keV, 100-200 keV (these are the energy ranges used in Ukwatta et al. 2010, for timing analysis).

4.3. *Timing Analysis*

The GRB was detected in the wide band of 26 keV to 1000 keV with both the *RT*-2 detectors. Since the GRB is incident at a large incident angle, meaningful light curves were available from the CsI(Tl) detectors in different energy bands (26-59 keV, 59-215 keV, and 215-1000 keV ranges for *RT*-2/S and 26-59 keV, 59-215 keV, 215-330 keV, and 330-1000 keV ranges for *RT*-2/G). The light curves, obtained from *RT*-2 and BAT instruments, are shown in Figure 1 with a bin time of 1 s and and the time is given with respect to the BAT trigger time T_0 of 2009 June 18 08:28:29 UT. The BAT light curves are in the units of mask-weighted counts, which are essentially background subtracted counts per fully illuminated detector for an equivalent on-axis source. The *RT*-2 count rates are the combined light curves from *RT*-2/S and *RT*-2/G detectors and they are normalized to the nominal detector area of 100 cm^2 for each detector. The light curves are arranged with increasing energy (from the top) and wherever possible light curves of comparable energy are plotted together (25 – 50 keV BAT data and 26 – 59 keV *RT*-2 data in panel b and 100 – 200 keV BAT data and 59 – 215 keV *RT*-2 data in panel c). For clarity, the 59 – 215 keV light curve from *RT*-2 is scaled down by a factor of 10 and vertically shifted up by 0.1 count s^{-1}.

The burst profile was found to be having a complex structure. The entire burst episode lasted for about 150 s with the brightest pulse detected at T_0 + 65 s. The other two weak emissions are registered at T_0 + 85 s and at T_0 + 115 s with low intensity. Another instrument, Konus-RF onboard the Coronas-Photon satellite, also detected the GRB 090618 with an identical burst profile (Golenetskii et al. 2009). The burst profile is not clearly detected in the lowest energy band of *RT*-2 (26 - 59 keV), whereas in the high energy X-rays, burst is detected with significant emission. There is a very significant softening of the spectrum in the precursor with the 25 – 50 keV light curve peaking several seconds after the high energy light curves. The main pulse at T_0+65 s shows a double structure, the 50 – 100 keV BAT profile showing a close similarity to the 59 – 215 keV *RT*-2 light curve. The pulse at T_0+85 s shows a single smooth structure in the 100 – 200 keV (similar to the 59 – 215 keV *RT*-2 light curve), with an indication of multiple structures in the low energies.

We have attempted to model the pulse with FRED profile developed by Kocevski et al. (2003). The empirical relation for the flux (photon counts s^{-1}) distribution is given by,

$$F(t) = F_m(\frac{t}{t_m})^r[\frac{d}{d+r} + \frac{r}{d+r}(\frac{t}{t_m})^{(r+1)}]^{-(r+d)/(r+1)}, \quad (1)$$

where, F_m is the maximum flux at t_m, r and d are the rising and decaying indices, respectively. First we fit the total light curves (26 – 1000 keV for *RT*-2 and 15 – 200 keV for BAT). The start times for fitting (for each pulse) were kept fixed at $t_m - t_{st}$, where t_{st} were varied between 15 s and 25 s. Since there were negligible changes in

the derived parameters, particularly for the measurement of width, we kept t_{st} fixed at 25 s. The reduced χ^2 for the *RT*-2 data is 1.38 (for 75 dof). For the higher sensitivity BAT data, however, the FRED profile does not take into account the sub-structures in the pulses, and hence formally unacceptable fits (reduced $\chi^2 \geq 10$), were obtained. Since our main emphasis is to find the broad pulse characteristics, we give below the parameters obtained from a FRED fitting. Further, we find that the derived parameters for the pulses 1 & 2 from the BAT data (these two pulses have a large overlap) are quite sensitive to the initial parameters used for fitting and hence the quoted formal errors could be underestimates.

The resultant derived parameters, along with the nominal 1-σ errors (obtained from the criterion $\Delta\chi^2 = 2.7$), are given in Table 1. There is a reasonable agreement in the derived parameters, obtained from *RT*-2 and BAT data. While fitting, an upper bound of 1000 is kept for the parameter d (for $d >> r$, F(t) becomes independent of d). We have measured the pulse width as the FWHM value of the fitted light curve. The fitted light curves with burst profiles are shown in Figure 2 for the total energy band of 26 to 1000 keV for the *RT*-2 detectors (bottom panel) and for the total energy band of 15 – 200 keV for the BAT detector (top panel). The fitting procedure is repeated for light curves of different energies. The times of the maximum emission t_m, however, were kept fixed at those values obtained from the fitting for the full energy light curves, of the respective detectors (*RT*-2 and BAT). The value of t_m could depend on energy upto about a second for these energies (see the delay analysis presented later), which might result in a further systematic error in the width measurement of < 1 s. We have plotted the width as function of mean energy in Figure 3. Mean energies are calculated as the mean energy of incident photons in the detector, based on the response function of the detectors, and they are derived to be 125.62 keV, 266.6 keV, and 427.5 keV, for the 59 – 215 keV, 215 – 330 keV, and 330 – 1000 keV bands, respectively for the *RT*-2 data. The mean energies for the four energy bands of BAT data are 20.82 keV, 35.45 keV, 68.07 keV, and 123.73 keV, respectively.

The first two pulses have similar profiles in both data sets, though in the *RT*-2 data the first pulse is much stronger than the second. There is an indication of further sub-structures in the BAT data which is not very apparent in the *RT*-2 data, possibly due to the lower sensitivity. The width decreased monotonically with energy. Also, there is a trend of steepening of this trend for the latter pulses, particularly for the third pulse. For example, by defining a width index ξ such that $width \propto E^{-\xi}$ (Fenimore et al. 1995), we find ξ to be 0.18, 0.07, 0.14 and 0.05, respectively for the four pulses, for a combined fit to the *RT*-2 and BAT data. These parameters are summarized in Table 3.

To investigate the softening of the spectra, we have performed cross correlation analysis between the light curves of various energies using the BAT data. We have taken the 15 – 25 keV as the base energy. Cross correlation is done for the full light curves as well as in parts: the first part includes the precursor (T_0 to T_0+50), the second part includes pulse 1 and 2 (T_0+50 to T_0+77) and part 3 and 4 include pulses 3 and 4, respectively. We have used the utility *crosscor* of the XRONOS software package (a part of the HEASOFT software package of HEASARC) to derive the cross correlation function (CCF) with respect to lag. A Gaussian function was used to fit the CCF and measure the time lag and the error is estimated using the criteria $\Delta\chi^2$=4.0 (see Dasgupta & Rao 2006). The results of cross correlation analysis are given in Table 2. We found soft lags which show clear energy dependence. The measured lag increases with energy and they are shown in Figure 4. There is also a tendency for this steepening to be flatter for the latter pulses. Defining a delay index d_i such that $delay = a + d_i ln(E)$, where a is a constant, we find d_i to be very steep for the precursor (-3.71) and it increased from -0.50 for Part 2 (pulses 1 & 2) to -0.13 for Part 3 (pulse 3). For the fourth part (pulse 4), however, d_i is found to be -0.92. The values of ξ and delay index (d_i) are compiled in Table 3.

Ukwatta et al. (2010) have derived delays for the light curve of T_0+46.01 to T_0+135.35 s as -0.171 s, -0.314 s and -0.579 s, respectively, in three energy bands given in Table 3, which is close to the average values of delays for part 2 and 3 (T_0+50 to T_0+100 s) reported in Table 3 (-0.247 s, -0.365 s, and -0.630 s, respectively, for the three energy bands). We have followed a method of cross-correlation analysis similar to that followed in Ukwatta et al. (2010) and we have confirmed that we get consistent results in the time span used in their work.

4.4. *Spectral Analysis*

We have analyzed the spectral data during the GRB event. It showed the typical Band spectrum with peak energy at about 164 keV and integrated 20 keV - 1 MeV fluence of 2.8×10^{-4} ergs cm^{-2}. We used 15-200 keV BAT data and the 100 – 650 keV *RT*-2 data of the GRB 090618 to perform joint spectral fitting.

The spectral information was available in the *RT*-2 data, every 100 s. The output from each detector is passed through two amplifiers of different gains (G1 and G2) and spectral data were available for each of the amplifiers: 1024 channel spectra for G1 (covering the energy range of 26 – 215 keV for the CsI detector) and 256 channel spectra for G2 (covering the energy range of 215 – 1000 keV). The number of channels are suitably rebinned for the spectral fitting.

RT-2/S and *RT*-2/G detectors are essentially collimated Phoswich detectors user for solar flare studies (Debnath et al. 2010). The shielding used for these detectors, however, are optimized to use them for hard X-ray spectroscopic studies of solar flares in 15 – 100 keV region and as omni-directional hard X-ray/gamma-ray detectors between $\sim$ 50 keV to 1000 keV (Sarkar et al. 2010). GRB 090618 is incident at an angle of 77°, and we have used a Monte Carlo (MC) simulation technique using the GEANT4 toolkit to derive the spectral response of the *RT*-2 detectors for this large incident angle (see Sarkar et al. 2010 for details). We created a mass model of the detector including all parameters like detector sizes, collimator, shield materials and mechanical support structures. Incident photons are used for the simulation in the energy range of 1 – 1000 keV in 50 equal bins in log scale and 10^5 photons in each bin are considered. The number of photons registered in the detectors as a function of energy is normalized to the incident photons for a GRB model with the spectral parameters of α = -0.32, β = -5.0 and E_0 = 67.7 keV. The

results are insensitive to model parameters (see later). This normalization is deemed as the effective area of the detectors. The derived effective areas for the NaI and CsI detectors are shown in Figure 5. Since the effective area of CsI is about an order of magnitude larger than the NaI detector, we have taken only the CsI data (and the corresponding response function) for our spectral fitting. The response matrix for the *RT*-2 detectors are generated using the *genresp* tool of *ftools*. The channel-energy conversion is derived from the background spectral line at ∼58.0 keV (Nandi et al. 2009) and 122 keV line due to the onboard calibration source (Co^{57}) and the energy resolution function is taken from the ground calibrations. Using this response matrix, a joint fit to the *RT*-2 and BAT data is performed. From the derived best fit spectral parameters, MC simulation is again carried out and the *RT*-2 response matrix is again created. Convergent results were obtained in the first trial itself, indicating that direct blocking from the surrounding material and interaction with detector play a major part of the response and the second order effects like scattering are unimportant for response matrix generation, at least to the level of sensitivity achieved for GRB 090618.

Except for a 2 mm aluminum filter in *RT*-2/G, both the detectors are identical in performance. The setting for deriving the onboard counts in the high energy channels is lower in *RT*-2/S and hence we have a single energy bin above 215 keV in *RT*-2/S (compared to the two energy bins in *RT*-2/G). Though we get consistent spectral results for both the detectors, we report the spectral parameters derived from *RT*-2/S which has better spectral response above 100 keV. While making a simultaneous fit to the BAT data, we kept the relative area between *RT*-2 and BAT as a free parameter and it is derived to be 1.30 for the combined fit to the full data. The relative area between *RT*-2 G1 and G2, however, is kept fixed at what is dictated by the response matrix. For the time resolved spectral fit the relative area between *RT*-2 and BAT is kept fixed at the value obtained for the full data (i.e., 1.30).

The spectrum can be well fitted with the model introduced by Band et al. (1993). In this model, two power-laws are smoothly joined at $(\alpha - \beta)\mathrm{E}_0$, where α is the first power-law index and β is the second power-law index, and E_0 is the break energy. The best fit spectral parameters are given in Table 3, along with the calculated peak energy E_p $(= \mathrm{E}_0\ (2 + \alpha))$ and the best fit χ^2 and the degrees of freedom used for the fitting. Figure 6 shows the best fit model along with the unfolded spectrum. We divided the BAT data in 4 parts and for each part we perform the spectral analysis. Since *RT*-2 does not have time-resolved spectral data, we have used the count rates as broad spectral data for this time-resolved spectral analysis. The results are shown in Table 3. Timing analysis parameters (width index ξ and delay index d_i) are also given in Table 3. We note that the spectral results agree quite well with that obtained from the *fermi* data (Ghirlanda et al. 2010). The values of E_p, derived in the present work, are 264 keV, 248 keV, 129 keV, and 33 keV respectively for the four parts which compares well with the value of 296 keV, 319 keV, 180 keV, and 81 keV derived for the peak of the light curves in these regions in the *fermi* data (time ranges, after T_0, of 3 – 14 s, 63 – 67 s, 80 – 85 s, and 114 – 130 s, respectively).

5. DISCUSSION AND CONCLUSIONS

In this paper, we have presented a method to measure the spectral parameters of the prompt emission using the recently launched *RT*-2 detectors and the Swift-BAT. Though *RT*-2 has been made to primarily study solar activities, we find that above ∼ 50 keV, *RT*-2 essentially acts as an all sky hard X-ray monitor. Thus, it can be used to measure the spectral and timing characteristics of the prompt emission of GRBs.

GRB 090618 shows multiple peaks. It shows a systematic softening of the spectrum for the successive pulses which is associated with the variations in the timing parameters. For the successive peaks in the GRB, the peak energy shifts to lower values, the width of the pulse varies sharply with energy and the delay (which is lower for the latter pulses) as a function of energy shows a flatter dependence on energy. The parameter ξ, characterizing the dependence of the pulse width with energy, also shows a strong pulse (and hence time) dependence.

Fenimore et al. (1995) used the width of individual pulses in several GRBs detected by BATSE and showed that the dependence on energy is a power-law, with an index of ∼0.4. Borgonovo et al. (2007) measured the width of several GRBs of known redshifts and found that ξ shows a continuous distribution. A large number of bursts in their work show ξ to be peaking around 0.1 – 0.2. It appears that GRB 090618 belongs to this class of GRB with a narrow distribution of ξ. Interestingly, though the value of ξ changes from pulse to pulse in this GRB, it is in the range of 0 – 0.1.

Various explanations are offered to understand the lags seen in GRBs. Shen et al. (2005) have estimated the contributions from the relativistic curvature effect. These effects can explain contributions to the lag of the order of 10^{-2} – 10^{-1} s. The lags observed in GRB 090618 is much larger than this and hence quite unlikely to be due to the curvature effect. Ioka & Nakamura (2001) have computed the kinematic dependence of lag caused by the viewing angle which could produce the observed dependences. The systematic pulse-to-pulse variation of the properties detected in GRB 090618, however, would be difficult to understand in this framework. Spectral evolution, too, can reproduce some part of the lag (Kocevski & Liang 2003; Hafizi & Mochkovitch 2007). The results from the present observations support the conclusion of Hakkila et al. (2008) that the spectral lags are pulse rather than burst properties.

The individual pulses in a GRB could be either due to emission from multiple shock locations when a jet material encounters the supernova ejecta or due to the weakening of the relativistic matter and/or the emission of a fresh relativistic matter from the central engine. Detection of properties of a GRB pulse quite different from the previous pulses has implications for the nature of the central engine. If the central engine is shown to emit multiple ejection episodes it will strongly favor a black hole as the candidate as against a highly magnetized neutron star (see for example, Metzger 2010 for a discussion on the GRB central engines). In the case of GRB 090618, there is a marginal evidence for the last pulse (pulse 4) to be different and could be a candidate for a separate emission from the central engine. A detailed study of

several such multi-peaked bursts are required to draw a firm conclusion. For example, discovery of a hard GRB pulse, after a X-ray pulse, would certainly favor a black hole as a candidate for the central engine.

We have calculated the isotropic energy (E_{iso}) for this GRB by considering a standard cosmology model for a flat universe with $q_0 = 1/2$ and $H_0 = 70$ km s^{-1} Mpc^{-1}. Using the measured redshift of 0.54 and the measured integrated fluence in the energy range of 20 keV to 1 MeV of 2.8 x 10^{-4} ergs cm^{-2}, we calculate E_{iso} to be 2.21 $\times$ 10^{53} ergs (beaming effects are neglected). The measured time-averaged peak energy (E_p) for the entire burst is around 164 keV, which gives the intrinsic peak energy ($E_{p,i}$) of 252 keV. Based on the measured values of $E_{p,i}$ and E_{iso}, it is found that the GRB 090618 closely follows the 'Amati' relation with a minor deviation, which is within the 2σ scatter. Hence, it could be concluded that GRB 090618 is a standard candle for the category of long duration GRBs alongwith various intrinsic properties that are discussed in this paper.

The recent detection of polarization in GRB 090102 (Steele et al. 2009) indicates the presence of ordered magnetic field in the source of GRBs during the prompt emission. The present measurement of the spectral and temporal parameters of GRB 090618 shows that the individual pulses show distinct behaviors.

This work was made possible in part from a grant from Indian Space Research Organization (ISRO). The wholehearted support from G. Madhavan Nair, Ex-Chairman, ISRO, who initiated the *RT*-2 project, is gratefully acknowledged. Significant contributions from several organizations for the realization of the *RT*-2 payload is gratefully acknowledged. This research has made use of data obtained through HEASARC Online Service, provided by the NASA/GSFC, in support of NASA High Energy Astrophysics Programs. We thank the anonymous referee of this paper for the very detailed comments which helped in improving the quality of the paper.

REFERENCES

Amati, L., et al. 2002, A&A 390, 81
Band, D., et al. 1993, ApJ, 413, 281
Barthelmy, S. D. et al., 2005, Space Sci. Rev., 120,143
Borgonovo, L., Frontera, F., Guidorzi, C., Montanari, E., Vetere, L., Soffitta, P. 2007, A&A, 465, 765
Burrows, D.N., et al., 2005, Space Sci. Rev., 120, 165
Baumgartner, W. H., et al., 2009, GCN Circ. 9530
Beardmore, A. P., et al., 2009, GCN Circ. 9528
Cenko, S. B., et al. 2009a, GCN Circ. 9513
Cenko, S. B., et al. 2009b, GCN Circ. 9518
Dado, S., & Dar, A. 2010, ApJL, 708, L112
Dar, A. 2006, ChJAS, 6, 301.
Dasgupta, S., & Rao, A. R. 2006, ApJ, 651, L13
Debnath, D. et al. 2010, Exp. Astron., (in press).
Evans, P. et al., 2009, GCN Circ. 9521
Fenimore, E. E., in't Zand, J. J. M., Norris, J. P., Bonnell, J. T., Nemiroff, R. J. 1995, ApJL, 448, 101
Golenetskii, S., et al., 2009, GCN Circ. 9553
Gehrels, N., et al. 2004, ApJ, 611, 1005
Gehrels, N., Ramirea-Ruiz, E., Fox, D.B. 2009, ARAA, 47, 567.
Ghirlanda, G., Nava, L., Ghisellini, G. 2010, A&A, 511, 43
Hafizi, M., Mochkovitch, R. 2007, A&A, 465, 67
Hakkila, J, Giblin, T. W., Norris, J. P., Fragile, P. C., Bonnell, J. T. 2008, ApJL, 677, L81
Ioka, K, Nakamura, T. 2001, ApJL, 554, L163
Klebesadel, R. W., Strong, I. B., Olson, R. A. 1973, ApJL, 182, 85
Kocevski, D., & Liang, E. 2003, ApJ, 594, 385
Kocevski, D., Ryde, F., & Liang, E. 2003, ApJ, 596, 389
Kono, K., et al. 2009, GCN Circ. 9568
Kotoch, T. et al. 2010, Exp. Astron., (in press)
Kotov, Yu., et al. 2008, In 37th COSPAR Scientific Assembly, in Montréal, Canada., p.1596
Longo, F., et al. 2009, GCN Circ. 9524
Lu, R.-J., Qin, Y.-P., Zhang, Z.-B., Yi, T.-F 2006, MNRAS, 367, 275L
Lyutikov, M. 2006, New Journal of Physics, 8, 119
McBreen, S., et al. 2009, GCN Circ. 9535
Meszaros, P. 2002, ARAA, 40, 137.
Metzger, B.D. 2010, arXiv:1001.5046
Nandi, A. et al., 2009, In Proc. of International Conference on Space Technology, Greece, G. Lampropoulos and M. Petrou (Eds.), arXiv:0912.4126
Nandi, A. et al. 2010, Exp. Astron., (in press).
Norris, J. P., Marani, G. F., Bonnell, J. T. 2000, ApJ, 534, 248
Norris, J. P., Bonnell, J. T. Kazanas, D., et al., 2005, ApJ, 627, 324.
Perley, D. A., et al. 2009, GCN Circ. 9514
Piran, T. 2004, RvMP, 76, 1143.
Rao, A. R., et al. 2009, GCN Circ. 9665
Roming, P. W. A., et al. 2005, Space Sci. Rev., 120, 95
Rujopakarn, W., et al. 2009, GCN Circ. 9515
Sakamoto, T., et al. 2009, GCN Circ. 9534
Sarkar, R. et al. 2010, (submitted in Exp. Astron.).
Schady, P., et al. 2009a, GCN Circ. 9512
Schady, P., et al. 2009b, GCN Circ. 9527
Schady, P., et al. 2009c, GCN Report 232.1
Shen, R-F., Song, L-M., Li, Z. 2005, MNRAS, 362, 59
Sreekumar, S. et al. 2010, Exp. Astron., (in press).
Steele, A., Mundell, C. G., Smith, R. J., Kobayashi, S. & Guidorzi, C. 2009, Nature, 462, 767
Ukwatta, T. N., et al. 2010, ApJ, 711, 1073
Xiao, L. & Schaefer, B. E. 2009, ApJ, 707, 387
Zhang, B. 2007, CJAA, 7, 1

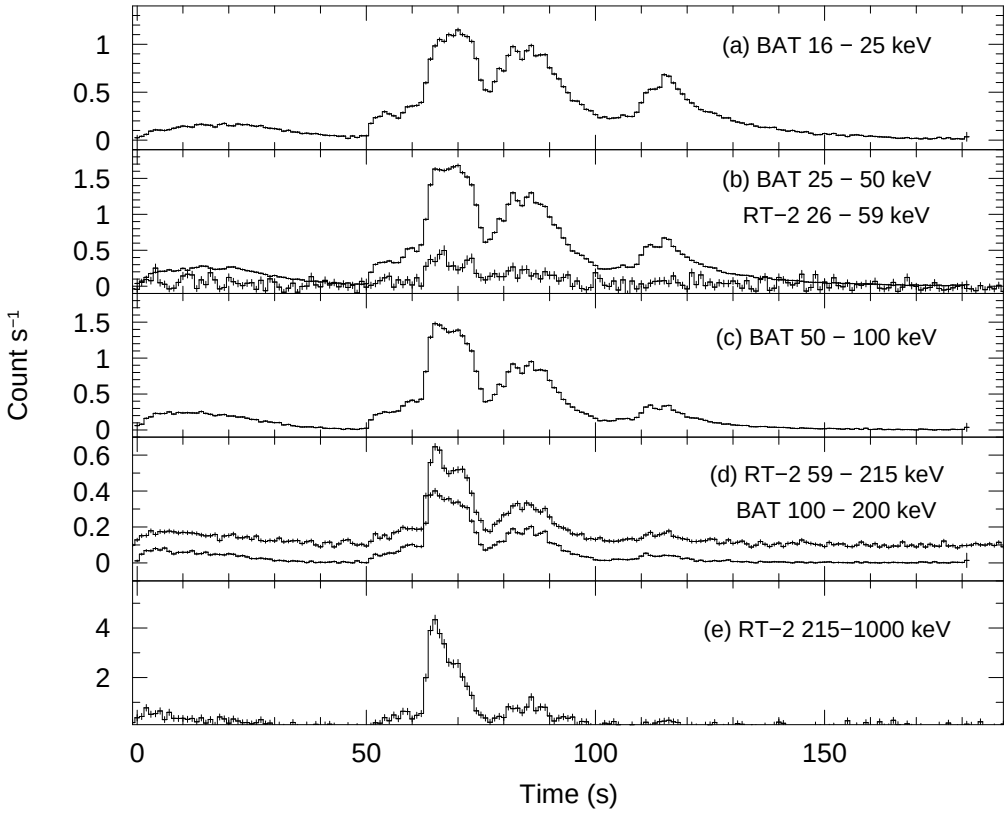

FIG. 1.— The light curves of GRB 090618 obtained from Swift/ BAT and the *RT*-2 experiments, with a bin time of 1 s. The BAT light curves are in the units of mask-weighted counts (see text). The *RT*-2 count rates are the combined light curves from *RT*-2/S and *RT*-2/G normalized to the nominal detector area of 100 cm^2 for each detector. For clarity, the 59 – 215 keV light curve from *RT*-2 is scaled down by a factor of 10 and vertically shifted up by 0.1 count s^{-1}. The time is given with respect to the BAT trigger time of 2009 June 18 08:28:29 UT.

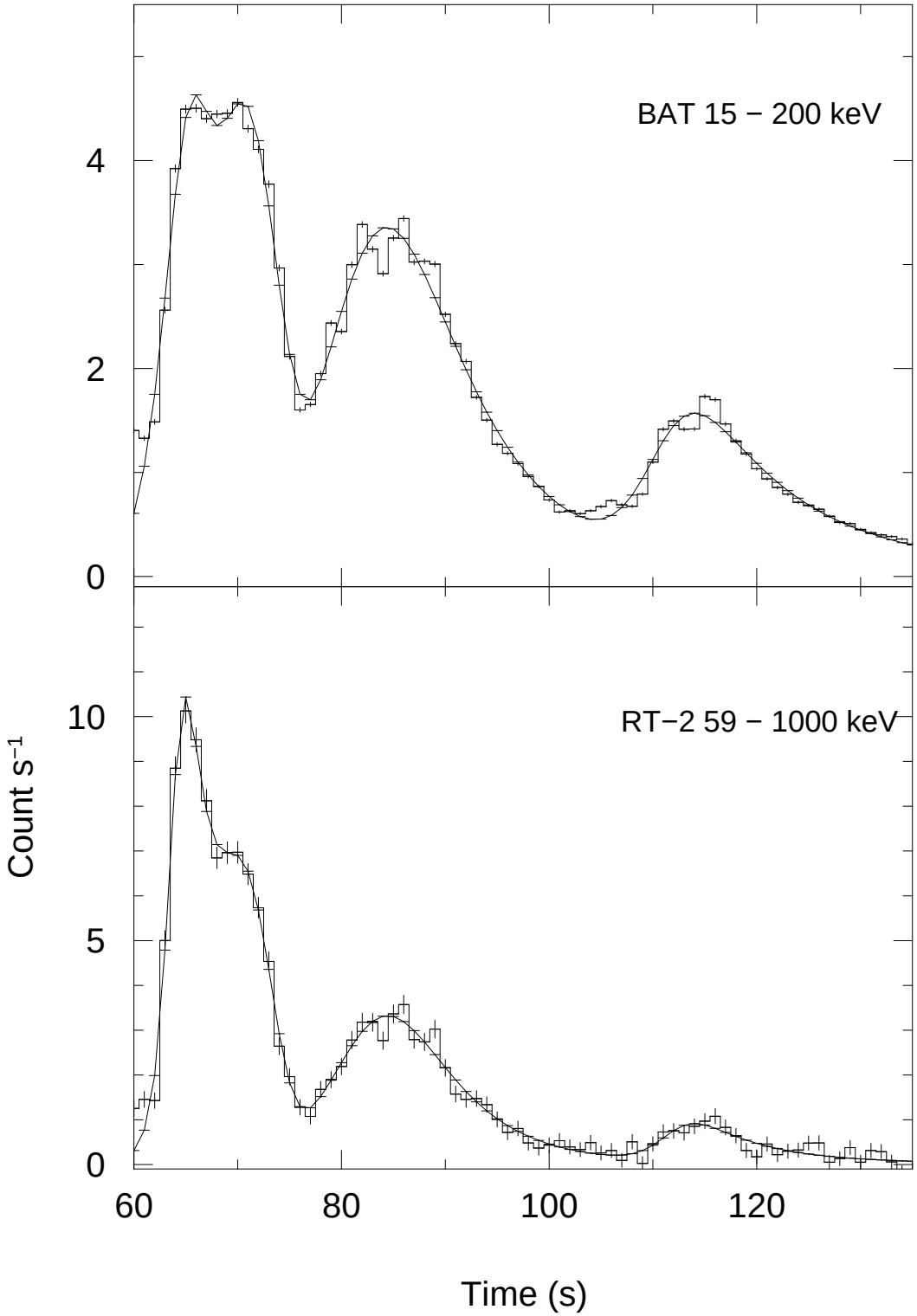

FIG. 2.— The light curves of GRB 090618 obtained from Swift/ BAT and the *RT*-2 experiments for the respective full energy ranges, shown along with a model consisting of four FRED profiles each. See Table 1 for the model parameters.

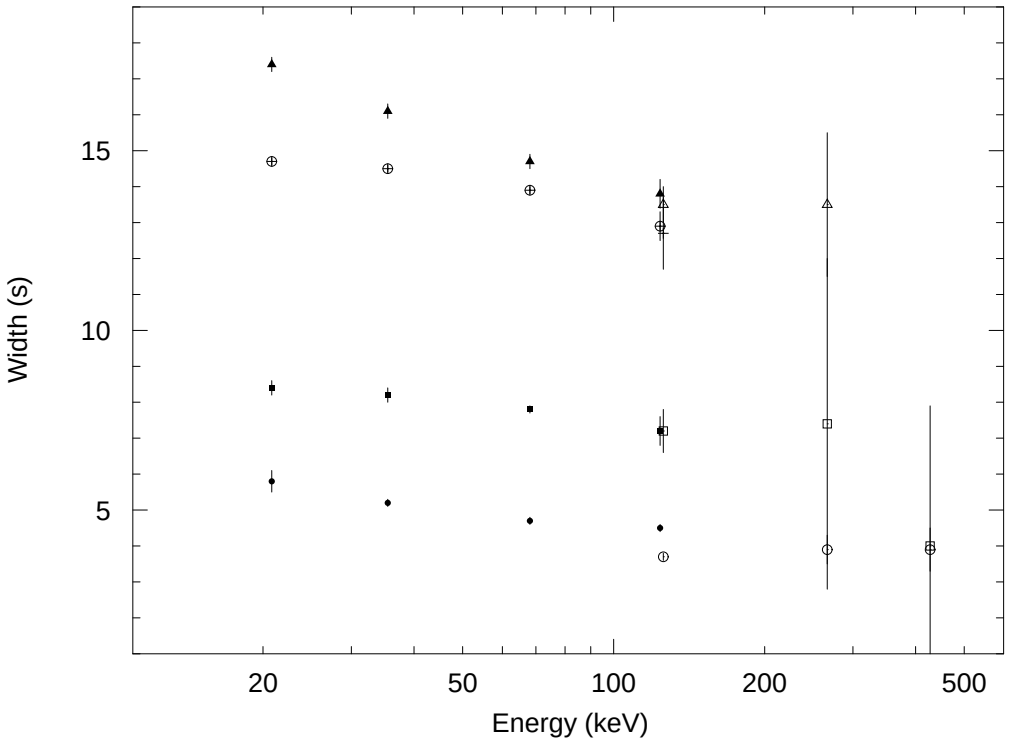

FIG. 3.— The pulse width variation as a function of average energy. For the four pulses (1 to 4, see text), data are plotted as filled circles, filled squares, filled triangles and circles with plus signs, respectively, for the BAT data and open circles, open squares, open triangles and circles, respectively, for the *RT*-2/G data.

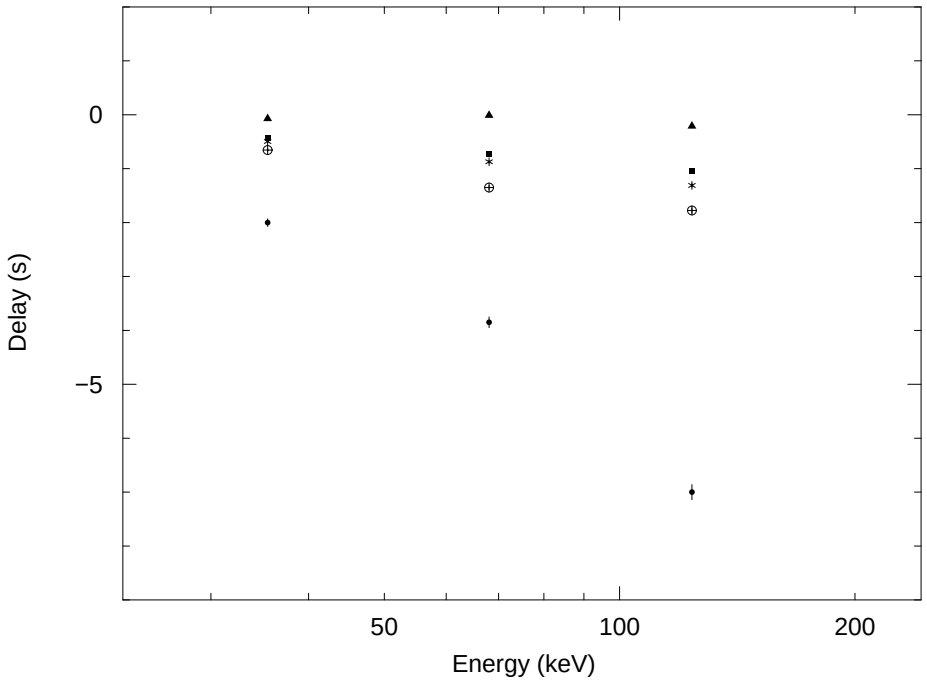

FIG. 4.— The measured delay of light curves with mean energy, E, with respect to the 15 – 25 keV light curve, plotted against E from the *Swift* BAT data. Data for the four parts (see text) and the total light curve are shown as filled circles, filled squares, filled triangles, circles with plus sign, and stars, respectively.

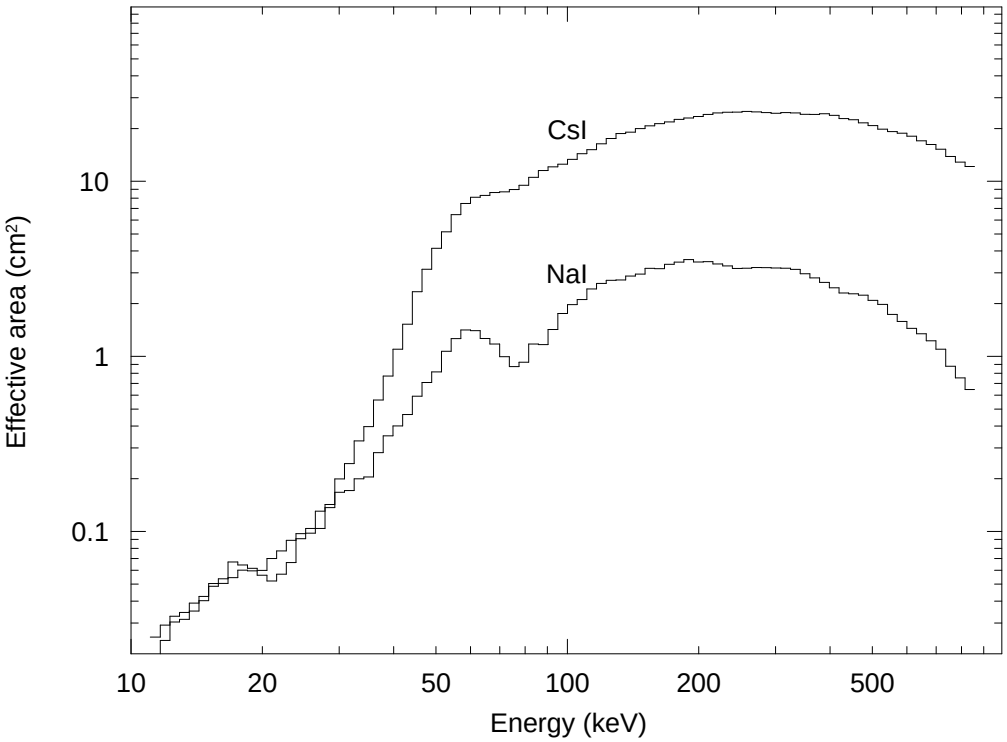

FIG. 5.— The effective area of *RT*-2 NaI(Tl) and CsI(Na) detectors, from a Monte Carlo simulation for the GRB incident at an angle of 77°.

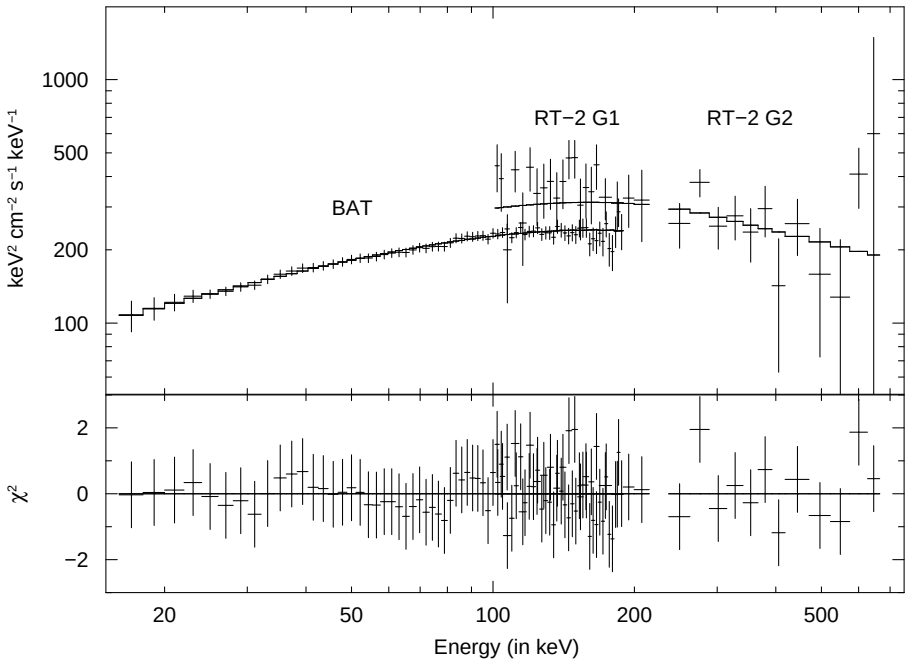

FIG. 6.— The unfolded spectrum (in energy units) of GRB 090618 using *Swift* BAT and *RT*-2 data, is shown along with the best fit model. The residuals are given in the bottom panel.

TABLE 1
PULSE CHARACTERISTICS OF GRB 090618

Pulse	Energy range (keV)	F_m (s^{-1})	t_m (s)	r	d	Width (s)
1	26 – 1000 (RT2)	8.7±0.8	64.8±0.2	27±4	15±5	3.9±0.3
2		5.9±0.7	70.5±0.3	8±1	1000	7.2±1.1
3		3.3±0.1	84.4±0.2	6±1	7±1	13.4±0.5
4		0.85±0.14	114.1±1.0	13±6	5±2	9.7±0.6
1	59 – 215 (RT2)	4.4±0.3	64.8	25±2	20±5	3.7±0.1
2		4.0±0.2	70.5	8±1	1000	7.2±0.6
3		2.3±0.1	84.4	6±1	7±1	13.5±0.5
4		0.6±0.1	114.1	8±3	5±2	12.7±1.0
1	215 – 330 (RT2)	2.8±0.4	64.8	29±5	14±6	3.9±0.4
2		1.5±0.4	70.5	8±4	895±35	7.4±4.6
3		0.76±0.11	84.4	6±3	8±6	13.5±2.0
1	330 – 1000 (RT2)	1.51±0.21	64.8	32±9	12±1	3.9±0.6
2		0.36±0.22	70.5	15±9	1000	4.0±3.9
1	15 - 200 (BAT)	2.80±0.03	65.0±0.1	13.6±0.4	39±4	5.0±0.1
2		4.31±0.03	70.5±0.1	7.0±0.1	1000	8.0±0.1
3		3.36±0.02	84.4±0.1	5.1±0.1	5.4±0.1	15.9±0.1
4		1.41±0.01	114.3±0.1	8.5±0.2	3.4±0.1	14.5±0.1
1	15 – 25 (BAT)	0.52±0.02	65.0	9.9±0.6	895±10	5.8±0.3
2		1.09±0.02	70.5	6.7±0.2	771±10	8.4±0.2
3		0.97±0.01	84.4	4.9±0.2	4.6±0.2	17.4±0.2
4		0.54±0.01	114.3	10.4±0.4	2.8±0.1	14.7±0.1
1	25 – 50 (BAT)	0.96±0.04	65.0	12.8±0.8	44±13	5.2±0.1
2		1.58±0.03	70.5	6.8±0.1	1000	8.2±0.2
3		1.28±0.01	84.4	5.1±0.2	5.3±0.2	16.1±0.2
4		0.54±0.01	114.3	8.5±0.3	3.4±0.1	14.5±0.1
1	50 – 100 (BAT)	0.99±0.03	65.0	15.5±0.8	30±6	4.7± 0.1
2		1.31±0.03	70.5	7.2±0.1	765±20	7.8± 0.1
3		0.93±0.01	84.4	5.4±0.2	6.2±0.2	14.7± 0.2
4		0.29±0.01	114.3	7.2±0.3	4.6±0.2	13.9± 0.1
1	100 – 200 (BAT)	0.31±0.02	65.0	18.1±1.6	23±7	4.5±0.1
2		0.31±0.02	70.5	7.9±0.5	900±50	7.2±0.4
3		0.19±0.01	84.4	5.2±0.4	8.5±1.0	13.8±0.4
4		0.04±0.003	114.3	6.1±1.1	6.4±1.5	12.9±0.4

TABLE 2
RESULTS OF CROSS-CORRELATION.

Division No.	energy bands	mean energy (keV)	Time lag (s)
Part1 (T_0 to T_0+50)	15-25 vs 25-50 keV	35.45	-2.0±0.07
	15-25 vs 50-100 keV	68.07	-3.85±0.10
	15-25 vs 100-200 keV	123.73	-7.00±0.14
Part2 (T_0+50 to T_0+77)	15-25 vs 25-50 keV	35.45	-0.424±0.026
	15-25 vs 50-100 keV	68.07	-0.721±0.030
	15-25 vs 100-200 keV	123.73	-1.050±0.035
Part3 (T_0+77 to T_0+100)	15-25 vs 25-50 keV	35.45	-0.070±0.04
	15-25 vs 50-100 keV	68.07	-0.010±0.03
	15-25 vs 100-200 keV	123.73	-0.210±0.033
Part4 (T_0+100 to T_0+180)	15-25 vs 25-50 keV	35.45	-0.655±0.030
	15-25 vs 50-100 keV	68.07	-1.349±0.040
	15-25 vs 100-200 keV	123.73	-1.775±0.052
Total (T_0 to T_0+180)	15-25 vs 25-50 keV	35.45	-0.495±0.026
	15-25 vs 50-100 keV	68.07	-0.872±0.028
	15-25 vs 100-200 keV	123.73	-1.310±0.035

TABLE 3
BEST FIT SPECTRAL PARAMETERS FROM A COMBINED FIT TO BAT AND *RT*-2 SPECTRA ALONG WITH TIMING PARAMETERS

Part	α	β	E_0 (keV)	χ^2/dof	E_p (keV)	ξ (*RT*-2 & BAT)	d_i
Full	-1.40±0.02	$-2.5^{+0.3}_{-0.5}$	273±31	56 / 101	164±24	–	-0.64
Part1 (precursor)	$-1.18^{+0.13}_{-0.08}$	< -1.6	322^{+176}_{-103}	52 / 55	264^{+209}_{-102}	–	-3.71
Part2 (pulse 1 & 2)	-1.23±0.05	< -2.1	322^{+79}_{-54}	56/ 55	248^{+81}_{-55}	0.18±0.03 & 0.07±0.03	-0.50
Part3 (pulse 3)	-1.39±0.03	-2.4±0.2	211^{+20}_{-11}	55/ 55	129^{+19}_{-13}	0.14±0.02	-0.13
Part4 (pulse 4)	$-1.70^{+0.07}_{-0.10}$	$-2.8^{+0.2}_{-1.1}$	111^{+20}_{-14}	37 / 55	33^{+15}_{-14}	0.05±0.01	-0.92